Deterministically fabricated strain-tunable quantum dot single-photon sources emitting in the telecom O-band (F)

N. Srocka, P. Mrowiński, J. Große, et al.

COLLECTIONS

Paper published as part of the special topic on Non-Classical Light Emitters and Single-Photon Detectors

(F)   This paper was selected as Featured

View Online   Export Citation   CrossMark

ARTICLES YOU MAY BE INTERESTED IN

Deterministically fabricated strain-tunable quantum dot single-photon sources emitting in the telecom O-band (F)

N. Srocka,[1] P. Mrowiński,[1,2] J. Große,[1] M. Schmidt,[1,3] S. Rodt,[1] and S. Reitzenstein[1,a] (iD)

AFFILIATIONS

[1]Institut für Festkörperphysik, Technische Universität Berlin, Hardenbergstraße 36, D-10623 Berlin, Germany
[2]Laboratory for Optical Spectroscopy of Nanostructures, Department of Experimental Physics, Wrocław University of Technology, Wybrzeże Wyspiańskiego 27, Wrocław, Poland
[3]Physikalisch-Technische Bundesanstalt, Abbestraße 2-12, 10587 Berlin, Germany

Note: This paper is part of the APL Special Collection on Non-Classical Light Emitters and Single-Photon Detectors.
[a]Author to whom correspondence should be addressed: stephan.reitzenstein@physik.tu-berlin.de

ABSTRACT

Most quantum communication schemes aim at the long-distance transmission of quantum information. In the quantum repeater concept, the transmission line is subdivided into shorter links interconnected by entanglement distribution via Bell-state measurements to overcome inherent channel losses. This concept requires on-demand single-photon sources with a high degree of multi-photon suppression and high indistinguishability within each repeater node. For a successful operation of the repeater, a spectral matching of remote quantum light sources is essential. We present a spectrally tunable single-photon source emitting in the telecom O-band with the potential to function as a building block of a quantum communication network based on optical fibers. A thin membrane of GaAs embedding InGaAs quantum dots (QDs) is attached onto a piezoelectric actuator via gold thermocompression bonding. Here, the thin gold layer acts simultaneously as an electrical contact, strain transmission medium, and broadband backside mirror for the QD-micromesa. The nanofabrication of the QD-micromesa is based on *in situ* electron-beam lithography, which makes it possible to integrate pre-selected single QDs deterministically into the center of monolithic micromesa structures. The QD pre-selection is based on distinct single-QD properties, signal intensity, and emission energy. In combination with strain-induced fine tuning, this offers a robust method to achieve spectral resonance in the emission of remote QDs. We show that the spectral tuning has no detectable influence on the multi-photon suppression with $g^{(2)}(0)$ as low as 2%–4% and that the emission can be stabilized to an accuracy of 4 μeV using a closed-loop optical feedback.

Published under license by AIP Publishing. https://doi.org/10.1063/5.0030991

The emission of single photons with controllable wavelength and high indistinguishability is a key parameter in quantum light sources for quantum nanophotonics. It is, for example, required to implement boson sampling experiments[1] and to realize entanglement swapping via Bell-state measurements in large-distance quantum communication networks based on the quantum repeater concept.[2–4] In fact, in the case of the quantum repeater, it is crucial to fabricate a chain of wavelength-tunable quantum light sources that provide identical photons on demand. Even more, it is important to operate such light sources at telecommunication wavelengths, i.e., within the telecom O-band ($\sim$1.3 μm) or C-band ($\sim$1.55 μm) with enhanced brightness[5] and a deterministic fabrication scheme,[6] to pave the way toward the real-world implementation of long-distance quantum communication networks via optical fibers, as recently reported using electrical Stark tuning of a quantum dot (QD) device.[7]

In this work, we demonstrate technological advances and experimental findings to realize wavelength-tunable quantum emitters of high single-photon purity in the telecom O-band. The strain-tunable emitters are based on self-assembled InGaAs quantum dots that are deterministically integrated into photonic nanostructures attached to piezoelements by means of a flip-chip process.[8,9] Here, the emission range of the InGaAs QDs is redshifted to the telecom O-band in the epitaxial growth process by using a strain-reducing layer (SRL),[10,11] while the piezoelectric actuator allows us to apply an external strain field to fine tune and stabilize the QD emission wavelength during operation of the quantum light sources. To demonstrate their

application potential, we examined the optical properties of two strain-tunable O-band single-QD mesa structures. The emission of their charged excitonic (CX) states, which are relevant for efficient single-photon generation,[12] is first studied regarding multi-photon suppression. Second, we test the wavelength tuning capabilities via strain-tuning and we introduce active spectral stabilization based on a closed-loop proportional–integral–derivative (PID) controller. Finally, we demonstrate strain-tuning and active stabilization of two remote QDs, which is a crucial step over existing results toward the real-world application of QD single-photon source (SPS) in advanced quantum communication schemes where it can pave the way toward two-photon interference (TPI) of remote sources in the telecom O-band required for the implementation of fiber-based quantum repeater networks.[4]

We manufactured our device in three main technological steps: (i) growing a semiconductor heterostructure by metal organic chemical vapor deposition, (ii) gold bonding an about 900 nm thick membrane of this structure onto a piezoelectric actuator, and (iii) nanostructuring the QD membrane deterministically by low-temperature cathodoluminescence (CL) scanning and *in situ* electron beam lithography (EBL).

First, a 200 nm GaAs buffer is grown on an n-doped GaAs (100) substrate followed by a 1 μm thick $Al_{0.90}Ga_{0.10}As$ etch stop layer, a 2 μm thick GaAs layer, and another 100 nm thick $Al_{0.90}Ga_{0.10}As$ layer. These three layers and the substrate are sacrificial layers to be removed during post-growth processing. The final 879 nm thick region of GaAs forms the active device membrane and includes a single InGaAs QD layer combined with the SRL, with the QD layer located 637 nm above the second etch stop layer [see Fig. 1(a)]. The QD layer is formed by 1.5 monolayers of $In_{0.7}Ga_{0.3}As$ followed by a 0.5 monolayer GaAs flush. The subsequent 5.5 nm thick InGaAs SRL has a gradual decrease in the In content from 30% to 10% over the first 3.5 nm.

Next, the as-grown sample and a PIN–PMN–PT [$Pb(In_{1/2}Nb_{1/2})O_3$–$Pb(Mg_{1/3}Nb_{2/3})O_3$–$PbTiO_3$] piezoelectric crystal are sputtered with 250 nm of gold. Their surfaces are then activated under argon plasma and, immediately after being removed from the deposition tool, bonded face-to-face under ambient air and thermocompression. In this step, a pressure of 6 MPa and a temperature of about 600 K are applied. This process allows for a stable bond that is not

affected by the inherent surface roughness of the PIN–PMN–PT crystal. For more details on this process, see Ref. 13.

The flip-chip process is finalized by a layer-by-layer wet-etching process. First, the 400 μm thick GaAs substrate is removed by a fast and aggressive etchant (H_2O_2/NH_3, 10:1) and stopped at the first $Al_{0.9}Ga_{0.1}As$ layer due to the high selectivity of the wet-chemical etching process.[14] HCl acid is then used to solely remove the exposed etch stop layer. In our process, we use HCl instead of the typically applied HF mainly because of the lower etch rate that leads to better process control and higher quality of the etched surfaces. The now-exposed second and thinner GaAs layer (2 μm) is lifted off by a slower etchant (citric acid/H_2O_2, 4:1), which leads to a significantly improved surface roughness compared to a single-step etch process. Again, the second etch stop layer is removed by HCL acid. At this point, an 885 nm thick membrane, containing the single QD layer, is gold bonded to a PIN–PMN–PT crystal and completely freed from sacrificial layers.

In preparation for the following main processing step, the sample is spin coated with a nominal 300 nm thick layer of AR-P 6200 (CSAR 62) electron-beam resist. The sample is then loaded in a special scanning electron microscope (SEM) that enables CL measurements at cryogenic temperatures. The sample is cooled to 10 K, and the CL signal is mapped over a 20 μm × 20 μm large area with a voxel size of 0.5 μm to identify the position of bright and isolated QDs that emit at the desired wavelength in the telecom O-band. A corresponding map showing spatially resolved CL in a spectral range of (1300–1305) nm is shown in Fig. 2(a). By applying a 2D Gaussian fit, we can select the two circled QDs in Fig. 2(a) with a lateral accuracy of about 40 nm. In the following electron beam lithography (EBL) step, deterministic circular mesa structures are written into the resist at low temperature (10 K) in the same SEM system. When the resist is developed, the image areas are cleared and only the EBL-structured mesa structures remain and form an etching mask for the final reactive ion etching in an inductively coupled plasma. For the circular QD micromesas with a gold mirror on the back, we expect a moderately high photon extraction efficiency η in the range of 5%–10%.[13,15] This parameter can possibly be increased in the future by applying the present manufacturing method to sources based on circular Bragg resonators (CBRs) that promise broadband photon extraction efficiency up to $\eta = 95\%$ in the telecom O-band.[16] In fact, our developed device processing is fully compatible with the realization of CBRs, and using a soon available commercial *in situ* EBL system, we plan to implement 1.3 μm QD-CBRs. In this context, it will be interesting to explore the effect of piezostrain tuning on both the QD and cavity properties, which could probably be used to induce a piezocontrolled slight ellipticity in the CBRs to realize high-performance QD-SPS with linearly polarized emission under resonant excitation.[17]

Noteworthily, and in contrast to previous work on piezoelectric tuning of QD-micromesas emitting in the 930 nm range,[18] the etching depth used in the present work corresponds to the thickness of the gold-bonded membrane in our design. Thus, the base diameter of the mesa structure is the only cross section to transfer the strain-field effect at the piezoelectric actuator to the QD position. As we discuss below, the limited contact area between the semiconductor and the piezoelectric actuator does not have a strong impact on the achievable tuning range, which is rather limited by non-ideal wafer-bonding.

The properties of the optical device are investigated by means of microphotoluminescence (μPL), μPL-excitation (μPLE), and
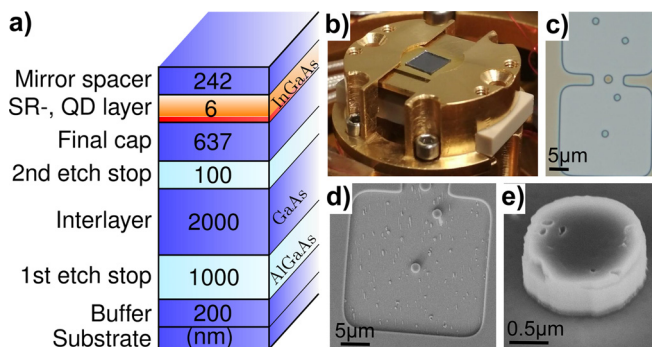
FIG. 1. (a) Sample structure as grown. (b) Sample mounted in the customized spring holder of the cryostat. (c) Optical microscope image of the sample after resist development. (d) SEM image of the processed sample showing the mapping area with the two mesas hosting QD1 and QD2. (e) SEM image of the investigated mesa hosting QD1.
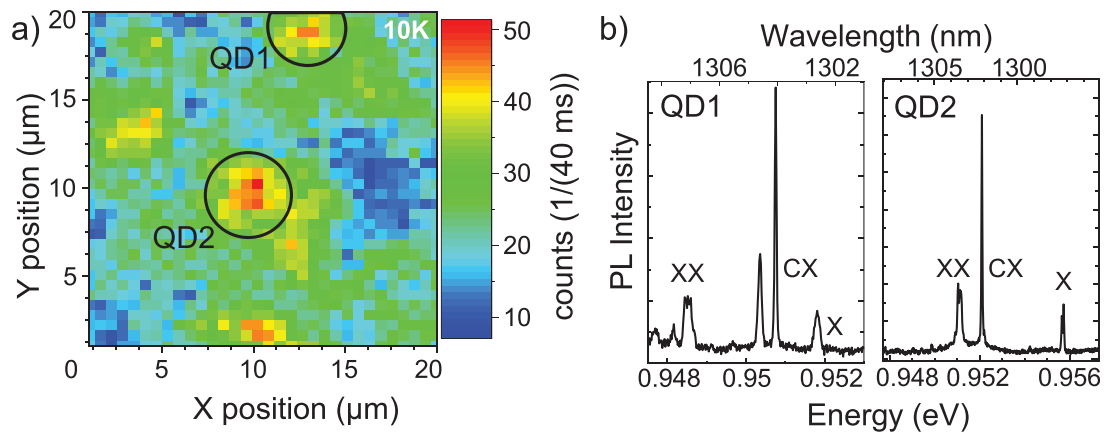
FIG. 2. (a) CL map of the pre-selection step at 10 K with QD1 and QD2 encircled. The spectral range of 1300 nm–1305 nm is depicted. (b) Corresponding μPL spectra of QD1 and QD2 after mesa processing was completed.

photon-correlation spectroscopy at 10 K. The used helium-flow cryostat has an extra-high-voltage feedthrough to electrically connect the piezoelectric actuator to a voltage supply and a customized spring holder to facilitate strain-tuning of the QD-micromesas. The deterministic QD mesa structures are optically excited by a continuous-wave (cw) diode laser (785 nm) or a tunable pulsed laser providing ps-pulses at a repetition rate of 80 MHz. The photoluminescence signal is collected with an objective [numerical aperture (NA) = 0.4] and spectrally resolved in a grating spectrometer (spectral resolution ∼20 μeV). The photon stream can either be detected by a liquid nitrogen cooled InGaAs-array detector or fiber-based Hanbury Brown and Twiss (HBT) and Hong–Ou–Mandel (HOM) configurations attached to the output slit of the monochromator. The quantum optical configurations include two superconducting nanowire single-photon detectors (SNSPDs) (a temporal resolution of approximately 50 ps and a detection efficiency of approximately 80% at 1310 nm).

Device characterization starts by basic μPL measurements under non-resonant cw excitation (785 nm) at 10 K. We identified two photonic structures with bright CX emission lines at 1303.98 nm (QD1) and 1303.78 nm (QD2). The spectral fingerprints of these two QDs, as shown in Fig. 2(b), have three characteristic and representative emission lines, which are identified as a neutral exciton (X), singly charged exciton (CX), and biexciton (XX) by excitation-power and polarization dependent measurements (see supplementary material Figs. S1 and S2).

To demonstrate strain-tuning and to quantify the corresponding spectral shift, the QD emission is studied depending on the applied voltage to the piezoelectric actuator. The applied voltage was varied from −400 V to +400 V, which corresponds to an electric field F of −13.4 kV cm^{-1} to +13.4 kV cm^{-1} and results in a spectral tuning range of 0.5 nm for the present sample, as shown in Fig. 3. Noteworthily, other samples showed a tuning range up to 4 nm when the device allows for applying higher voltages of up to ±33 kV cm^{-1} (cf. Fig. S3), however, at the risk of sample damage. Comparison between these results and values reported in Ref. 18 for a non-completely etched QD-mesa shows that the complete removal of the semiconductor material around the QD-mesa does not significantly reduce the available tuning range since in the electric field range

of ±20 kV/cm, the achieved relative spectral shift of (0.24 ± 0.02)% for device B presented in the supplementary material, which is consistent with (0.20 ± 0.02)% that can be extracted for the device discussed in Ref. 18. In fact, we observe strong device-to-device variations of the available tuning range, which indicates non-ideal wafer-bonding using our home-made bonding tool, and we expect higher tuning ranges and better reproducibility by using a commercial wafer bonder in the future.

In addition to the desired wavelength shift of our piezocontrolled QD-micromesas, we observe spectral fluctuation over time due to piezoelectric creep, which is most pronounced directly after a voltage change. To illustrate this point, Fig. 4(a) shows a systematic wavelength change of about 0.05 nm over the first 5 min after setting the piezovoltage. The creep effect decreases significantly after 30 min but does not vanish completely over time. This behavior is similar to
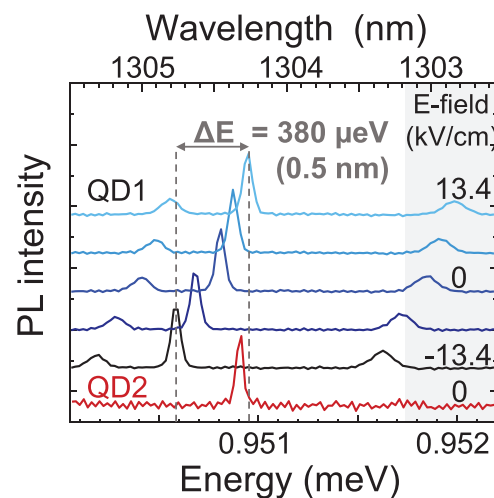
FIG. 3. Energy tuning of the CX emission line of QD1 (black to blue). An energy shift of 380 μeV (0.5 nm) was observed when changing the electric field applied to the piezoelectric actuator from −13.4 kV/cm to +13.4 kV/cm. The CX emission line of QD2 without the applied electric field (red) is within the energetic tuning limits of QD1.
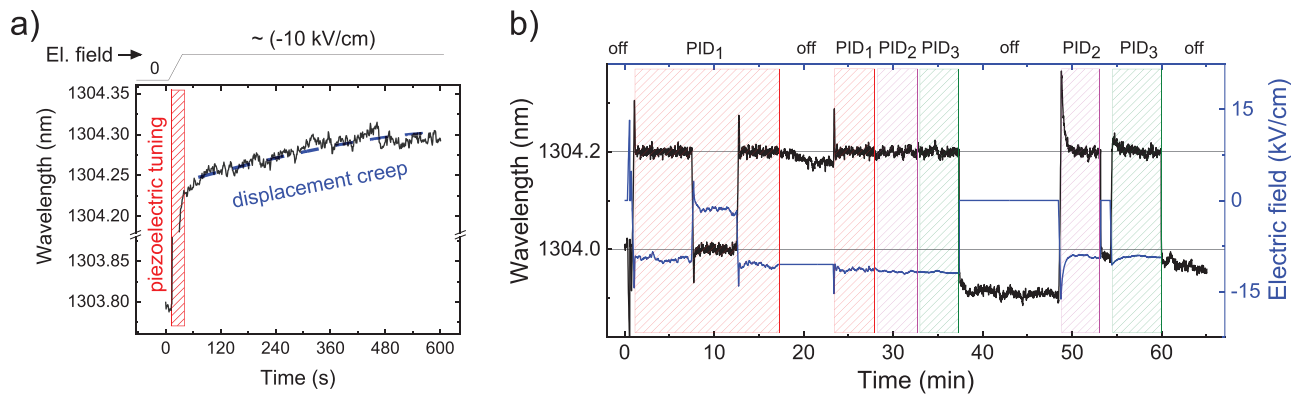
FIG. 4. (a) Impact of the piezoelectric actuator's creep on the wavelength of the CX emission line of QD1 over time. (b) PID stabilization tests on QD1 (see Table I for the summary).

earlier observations in piezocontrolled QD devices.[8,18,19] In addition, we examined the relative change of the emission energies of X, XX, and CX and we found that the binding energy is only slightly influenced, on a scale of 0.3 meV, by the applied strain (see supplementary material Fig. S3). This change in binding energy is significantly smaller than values on the order of meV observed for planar QD samples with obviously better strain transfer.[20] For some QDs, the excitonic fine structure splitting (FSS) could be reduced from 40 μeV to 20 μeV [see supplementary material Fig. S3(d)]. Further FSS reduction is not possible in our case. In fact, a second degree of freedom in the piezoelectric actuator would be required to fully symmetrize the distorted confinement potential, being responsible for the FSS.[21]

Long-term spectral stability is one of the most important aspects of a practical single-photon source for quantum communication applications based, e.g., on entanglement swapping via Bell-state measurements. Therefore, the effect of creep on the wavelength stability is an important issue to address. One can efficiently stabilize the emission wavelength, as it was reported for a quantum light emitting diode[8] and later also realized for a deterministically fabricated InAs/GaAs QD microlens,[18] by using an active optical feedback (closed-loop) algorithm. In the implemented concept, the emission wavelength is monitored by Lorentzian fitting of μPL spectra taken regularly within an integration time of 0.2–1.0 s, depending on the signal intensity. The center position of the fit is compared with the target wavelength, and the determined deviation initiates a re-adjustment procedure of the input voltage to shift the emission line back to the set target value. This re-adjustment is based on a PID algorithm.

The implemented wavelength stabilization is demonstrated for the CX emission of QD1 for several PID settings. In this test, we set the proportional gain (PG) to 100, and the integral time (IT) parameter to 0.01 s, 0.05 s, and 0.1 s to study its impact on the QD wavelength control after a voltage change applied to the piezoactuator. A graphical representation of the associated results is shown in Fig. 4(b), where the following settings are characterized within a time window of 5 min for each setting. The corresponding parameter set and achieved wavelength stability are shown in Table I. Evaluation of the recorded μPL time traces shows that the best spectral stabilization with a standard deviation of the emission wavelength (energy) of 5.6 pm (4.1 μeV) could be achieved for PG = 100 and IT = 0.01 s. Moreover, we found that by

increasing PG, the stabilization time decreases. However, in order to maintain the stabilization quality, the IT value must be increased proportionally. We did not observe any clear dependence of the QD spectral stability on the change in the derivative term of the PID controller.

Next, we demonstrate resonance tuning and stabilization of CX emission lines of the two different QD-micromesas (QD1 and QD2) by applying the optimized PID settings determined before. The time evolution of the piezoelectrically stabilized CX emission wavelength is presented in Fig. 5(a), showing standard deviations of 12 μeV for QD1 and 6 μeV for QD2, respectively. In Fig. 5(b), we present μPL spectra of both QDs tuned into resonance and being stabilized at 1304.05 nm with respect to the CX emission line. The good spectral overlap of the inhomogeneously (by spectral diffusion) broadened emission lines of QD1 and QD2 under active PID control reflects the efficient fine tuning and spectral control of the QDs via the PID controlled piezoactuator. Ultimately, it has to be demonstrated that a high spectral overlap can also be achieved on a scale of the homogenous linewidth, which can be probed by HOM experiments on remote sources.

To verify the quantum nature of emission, we measured the photon-autocorrelation of the spectrally tunable CX lines of QD1 and QD2. Here, the CX transition is driven at saturation under pulsed non-resonant excitation with a repetition rate of 80 MHz. In Fig. 6, we present histograms of the correlation events recorded in the HBT configuration representing the second-order autocorrelation function $g^{(2)}(\tau)$, which is used to evaluate the multi-photon suppression at zero time delay. First, the autocorrelation functions of QD1 and QD2 were measured without the influence of the piezoinduced strain-field emitting at different wavelengths, as shown in the upper panels of Fig. 6. The measurements show pronounced antibunching for the central

TABLE I. Quantified results of the emission energy stability for various PID integral times evaluated in terms of the standard deviation of emission energy and stabilization time required for the adjustment.

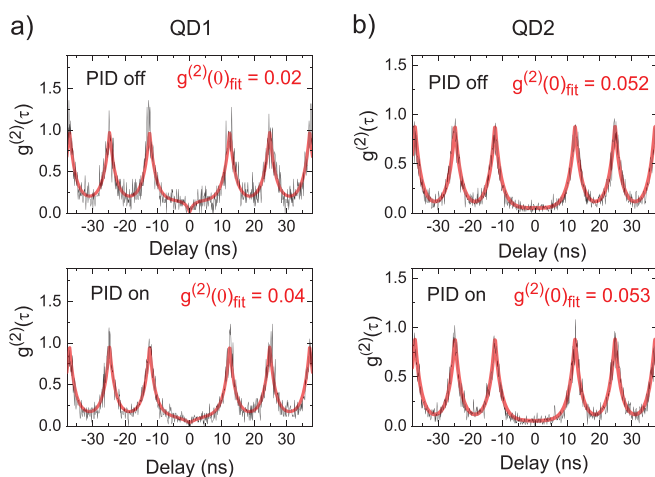| PID settings (prop. gain = 100)	PID$_1$	PID$_2$	PID$_3$
PID integral time (s)	0.01	0.05	0.1
Standard deviation (μeV)	4.12	4.45	5.26
Stabilization time (s)	30	50	80
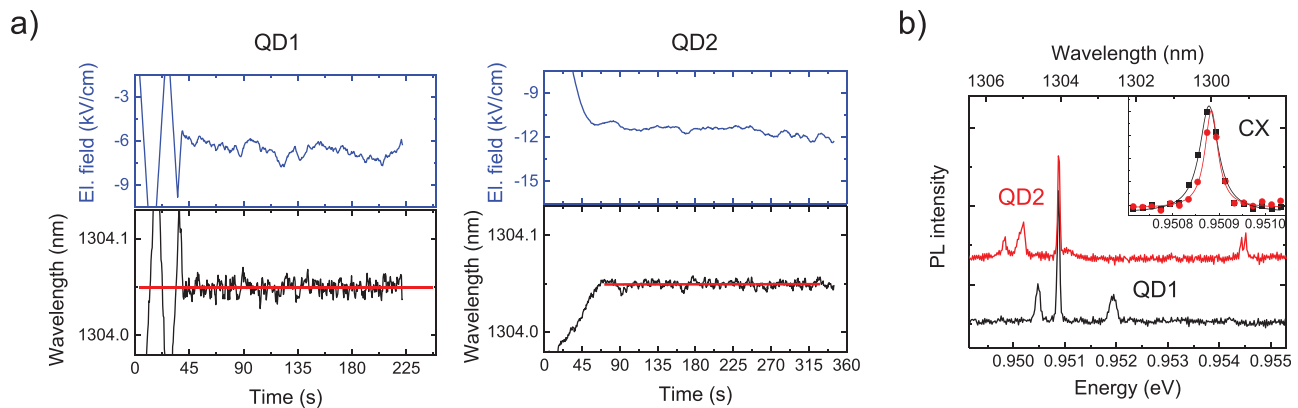
FIG. 5. (a) Emission wavelength traces of QD1 and QD2 over time to quantify the stabilization and (b) μPL spectra when both QDs are tuned in resonance via the applied piezoelectric strain field.

peak at $\tau = 0$ ns, and the evaluation of the experimental data with two-sided mono-exponential fit functions convoluted with the timing response of 50 ps of the SNSPDs used in this experiment yields $g^{(2)}(0)_{fit} = 0.020^{+0.030}_{-0.020}$ for QD1 and $g^{(2)}(0)_{fit} = 0.052 \pm 0.030$ for QD2. When the electric field is applied to the piezoactuator and both QDs' CX emissions are set to the resonant wavelength and stabilized by PID for several minutes at 1304.05 nm (the measurements were taken independently), the antibunching behavior is preserved and the corresponding fits yield $g^{(2)}(0)_{fit} = 0.040 \pm 0.030$ for QD1 and $g^{(2)}(0)_{fit} = 0.053 \pm 0.030$ for QD2, confirming that the spectral tuning has no significant impact on the single-photon purity of the QD-micromesas. The achieved results are very promising with regard to the target applications requiring the emission of indistinguishable single photons from remote quantum light sources. However, we would like to point out that the photon indistinguishability of these QD-micromesas is not yet high enough for this purpose. In fact, we

examined the TPI of tunable and stabilized CX emission of QD1 under pulsed p-shell excitation in the Hong–Ou–Mandel configuration. As we discuss in the supplementary material, this experiment yields a HOM visibility of $(16 \pm 8)\%$, a post-selected visibility of $(79 \pm 15)\%$, with a corresponding coherence time of (470 ± 85) ps, and a lifetime of $\tau_1 = (1.54 \pm 0.05)$ ns (see the supplementary material, Figs. 5 and 6). These values are in agreement with results achieved recently for non-tunable QD-micromesas,[13] which indicates that the optical quality and coherence of the 1.3 μm QD have to be improved in the future, e.g., by optimizing the SRL, in order to fully exploit their potential in advanced quantum communication applications. For instance, the gradual increase in the In content in the SRL and the overall thickness of the SRL could be varied as an optimization parameter to achieve a smoother transition from the strongly lattice mismatched $In_{0.7}Ga_{0.3}As$ QD layer to the GaAs matrix, thereby reducing the density of (charge trapping) defect states. Alternatively, one could also consider slowing down the GaAs growth on top of the SRL and try to better "heal" out the roughness introduced by the In-containing layers. HOM measurements can be a sensitive tool to evaluate the impact of design modifications on the optical and quantum optical properties of the 1.3 μm QDs.

In summary, we demonstrated a deterministically fabricated and tunable QD single-photon source emitting in the telecommunication O-band at 1.3 μm. Our device consisting of a QD micromesa and attached to a piezoelectric actuator allows us to fine tune the QD's emission wavelength by up to 0.5 nm via a voltage-controlled strain field. The tuning range and an implemented closed-loop PID control system enabled us to stabilize the emission energy with an accuracy (standard deviation) of up to $\sim$4 μeV and to hold emission lines of two remote QD-micromesas with multi-photon-suppression better than 5% in resonance with excellent spectral overlap. These results are very promising for the future implementation of long-distance quantum communication networks.

FIG. 6. (a) Autocorrelation experiments performed on the charged excitons of QD1 and (b) QD2 in the case of "on" and "off" PID controllers, which are used for stabilizing the piezocontrolled wavelength of the emitters.

See the supplementary material for information on the identification of excitonic complexes in QD1 and QD2, Hong–Ou–Mandel studies on the photon indistinguishability of QD1, and on optical properties of a second device with a larger strain-tuning range.

DATA AVAILABILITY

The data that support the findings of this study are available from the corresponding author upon reasonable request.

REFERENCES

[1]H. Wang, J. Qin, X. Ding, M. C. Chen, S. Chen, X. You, Y. M. He, X. Jiang, L. You, Z. Wang, C. Schneider, J. J. Renema, S. Höfling, C. Y. Lu, and J. W. Pan, Phys. Rev. Lett. **123**, 250503 (2019).

[2]P. Kok, C. P. Williams, and J. P. Dowling, Phys. Rev. A **68**, 022301 (2003).

[3]H. J. Kimble, Nature **453**, 1023 (2008).

[4]K. Azuma, K. Tamaki, and H.-K. Lo, Nat. Commun. **6**, 6787 (2015).

[5]J. Yang, C. Nawrath, R. Keil, R. Joos, X. Zhang, B. Höfer, Y. Chen, M. Zopf, M. Jetter, S. L. Portalupi, F. Ding, P. Michler, and O. G. Schmidt, Opt. Express **28**, 19457 (2020).

[6]M. Sartison, L. Engel, S. Kolatschek, F. Olbrich, C. Nawrath, S. Hepp, M. Jetter, P. Michler, and S. L. Portalupi, Appl. Phys. Lett. **113**, 032103 (2018).

[7]Z. H. Xiang, J. Huwer, J. Skiba-Szymanska, R. M. Stevenson, D. J. P. Ellis, I. Farrer, M. B. Ward, D. A. Ritchie, and A. J. Shields, Commun. Phys. **3**, 121 (2020).

[8]R. Trotta, P. Atkinson, J. D. Plumhof, E. Zallo, R. O. Rezaev, S. Kumar, S. Baunack, J. R. Schröter, A. Rastelli, and O. G. Schmidt, Adv. Mater. **24**, 2668 (2012).

[9]B. Höfer, F. Olbrich, J. Kettler, M. Paul, J. Höschele, M. Jetter, S. L. Portalupi, F. Ding, P. Michler, and O. G. Schmidt, AIP Adv. **9**, 085112 (2019).

[10]V. M. Ustinov, N. A. Maleev, A. E. Zhukov, A. R. Kovsh, A. Y. Egorov, A. V. Lunev, B. V. Volovik, I. L. Krestnikov, Y. G. Musikhin, N. A. Bert, P. S. Kop'ev, Z. I. Alferov, N. N. Ledentsov, and D. Bimberg, Appl. Phys. Lett. **74**, 2815 (1999).

[11]M. Paul, F. Olbrich, J. Höschele, S. Schreier, J. Kettler, S. L. Portalupi, M. Jetter, and P. Michler, Appl. Phys. Lett. **111**, 033102 (2017).

[12]S. Strauf, N. G. Stoltz, M. T. Rakher, L. a Coldren, P. M. Petroff, and D. Bouwmeester, Nat. Photonics **1**, 704 (2007).

[13]N. Srocka, P. Mrowiński, J. Große, M. von Helversen, T. Heindel, S. Rodt, and S. Reitzenstein, Appl. Phys. Lett. **116**, 231104 (2020).

[14]A. R. Clawson, Mater. Sci. Eng. R: Rep. **31**, 1 (2001).

[15]N. Srocka, A. Musiał, P.-I. Schneider, P. Mrowiński, P. Holewa, S. Burger, D. Quandt, A. Strittmatter, S. Rodt, S. Reitzenstein, and G. Sęk, AIP Adv. **8**, 085205 (2018).

[16]L. Rickert, T. Kupko, S. Rodt, S. Reitzenstein, and T. Heindel, Opt. Express **27**, 36824 (2019).

[17]H. Wang, Y. M. He, T. H. Chung, H. Hu, Y. Yu, S. Chen, X. Ding, M. C. Chen, J. Qin, X. Yang, R. Z. Liu, Z. C. Duan, J. P. Li, S. Gerhardt, K. Winkler, J. Jurkat, L. J. Wang, N. Gregersen, Y. H. Huo, Q. Dai, S. Yu, S. Höfling, C. Y. Lu, and J. W. Pan, Nat. Photonics **13**, 770 (2019).

[18]M. Schmidt, M. V. Helversen, S. Fischbach, A. Kaganskiy, R. Schmidt, A. Schliwa, T. Heindel, S. Rodt, and S. Reitzenstein, Opt. Mater. Express **10**, 76 (2020).

[19]T. Zander, A. Herklotz, S. Kiravittaya, M. Benyoucef, F. Ding, P. Atkinson, S. Kumar, J. D. Plumhof, K. Dörr, A. Rastelli, and O. G. Schmidt, Opt. Express **17**, 22452 (2009).

[20]F. Ding, R. Singh, J. D. Plumhof, T. Zander, V. Křápek, Y. H. Chen, M. Benyoucef, V. Zwiller, K. Dörr, G. Bester, A. Rastelli, and O. G. Schmidt, Phys. Rev. Lett. **104**, 067405 (2010).

[21]R. Trotta, J. Martín-Sánchez, J. S. Wildmann, G. Piredda, M. Reindl, C. Schimpf, E. Zallo, S. Stroj, J. Edlinger, and A. Rastelli, Nat. Commun. **7**, 10375 (2016).